Journal of Catalysis 258 (2008) 210–218

Contents lists available at ScienceDirect

Journal of Catalysis

www.elsevier.com/locate/jcat

Palladium–gallium intermetallic compounds for the selective hydrogenation of acetylene
Part I: Preparation and structural investigation under reaction conditions

Jürgen Osswald [a], Rainer Giedigkeit [b], Rolf E. Jentoft [a], Marc Armbrüster [a], Frank Girgsdies [a], Kirill Kovnir [a,b], Thorsten Ressler [c], Yuri Grin [b], Robert Schlögl [a,*]

[a] Department of Inorganic Chemistry, Fritz Haber Institute of the Max Planck Society, Faradayweg 4-6, 14195 Berlin, Germany
[b] Max-Planck-Institut für Chemische Physik fester Stoffe, Nöthnitzer Str. 40, 01187 Dresden, Germany
[c] Institute of Chemistry, Technical University Berlin, Straße des 17. Juni 135, 10623 Berlin, Germany

ARTICLE INFO

Article history:
Received 21 February 2008
Revised 5 June 2008
Accepted 13 June 2008
Available online 15 July 2008

Keywords:
Palladium
Gallium
PdGa
Pd_3Ga_7
Acetylene
Ethylene
Hydrogenation
Selectivity
Stability
Site isolation
Intermetallic compound
Hydride
XAS
XRD

ABSTRACT

The intermetallic compounds PdGa and Pd_3Ga_7 are introduced as selective catalysts for the hydrogenation of acetylene. Single phase PdGa and Pd_3Ga_7 can readily be prepared by the appropriate thermal treatment of the stoichiometric mixtures of the corresponding elements. The initial low surface areas of the as-prepared materials can be increased by careful mechanical treatment without decomposition. Detailed investigations of PdGa and Pd_3Ga_7 by DSC/TG, *in situ* powder X-ray diffraction and *in situ* X-ray absorption spectroscopy during thermal treatment under various inert or reactive gas atmospheres showed a high thermal stability. The long-range and short-range order in the crystal structures remained intact up to temperatures of about 600 K. Neither phase transitions nor decomposition were detectable. In addition to high thermal stability—preserving the active-site isolation under reaction conditions—no incorporation of hydrogen or carbon in the intermetallic compounds under reducing conditions was observed. Besides being interesting model systems, palladium–gallium intermetallic compounds are promising candidates for the application as highly selective hydrogenation catalysts.

1. Introduction

Catalytic hydrogenation of acetylene to ethylene ($C_2H_2 + H_2 \rightarrow C_2H_4$, $\Delta H = -172$ kJ/mol) is a common method for removing traces of acetylene in the feed for the production of polyethylene [1–3]. Acetylene is formed in small quantities during naphtha cracking and can lead to deactivation of the ethylene polymerization catalyst. To decrease the cost for polyethylene production, a selective and stable hydrogenation catalyst is required to reduce the amount of acetylene in the feed without hydrogenating a large fraction of ethylene. Palladium supported on metal oxides is a common highly active catalyst for this purpose but shows only limited selectivity and long-term stability [4,5]. In particular, highly active fresh or regenerated catalysts may exhibit overheating because of the exothermic reaction and, thus, a reduced selectivity, while deactivation of the catalyst by carbon deposition requires frequent exchange or regeneration of the catalyst.

Palladium metal provides spacious active sites enabling side reactions like oligomerization and full hydrogenation of acetylene to ethane [6]. In contrast to these reactions, the sequential hydrogenation of acetylene to ethylene via vinyl and vinylidene intermediates requires a decreasing active site size.

Catalyst surfaces that expose only isolated active-sites exhibit a reduced number of possible adsorption geometries. Acetylene molecules will preferably be weakly π-bonded and the amount of di-σ-bonded acetylene as well as adsorbed ethylene and ethylidyne species will be reduced [7–16], leading to a smaller amount of oligomerization products. Therefore, restricting the size of the active sites in a palladium containing hydrogenation catalyst and thereby preventing the formation of ensembles of neighboring Pd atoms on the surface—so-called *active-site isolation*—may increase the catalyst selectivity and long-term stability in acetylene hydro-

* Corresponding author.
E-mail address: acsek@fhi-berlin.mpg.de (R. Schlögl).

0021-9517/$ – see front matter
doi:10.1016/j.jcat.2008.06.013

genation. In addition to the presence of neighboring Pd atoms, the formation of palladium hydrides under hydrogenation reaction conditions substantially influences the selectivity. Reducing the amount of hydrogen incorporated in the catalyst diminishes the hydrogen supply for the hydrogenation reaction and increases the selectivity of acetylene hydrogenation to ethylene [17–24].

Using palladium alloys is one way to reduce the number of neighboring Pd atoms on the catalyst surface by simple dilution. Palladium–silver alloys [25], for instance, indeed exhibit an improved selectivity and stability compared to elemental Pd metal. However, a sufficient isolation of Pd atoms is difficult to attain without considerably decreasing the concentration of the active Pd constituent in the metal alloy catalyst. Moreover, surface segregation and Pd-ensemble effects may degrade the theoretical separation by random distribution of the Pd atoms in an metal alloy [26–31]. Therefore, it is desirable to find a material containing a sufficient amount of Pd together with another less expensive and catalytically inactive metal, and a well-defined crystal structure with the Pd atoms sufficiently isolated from each other. The well-ordered crystal structure clearly separates the intermetallic compounds—used in this study—from the alloys or bimetallic particles that were used in earlier studies, showing a random distribution of the different atoms on the lattice positions and varying compositions from one particle to another [32,33]. Pd-containing intermetallic compounds may fulfill the aforementioned requirements and, hence, may be promising candidates for improved hydrogenation catalysts. In order to verify the validity of this concept, the binary palladium–gallium intermetallic compounds PdGa and Pd_3Ga_7 were selected. They show the required structural (Figs. 1 and 2) and thermal properties. In addition, both materials possess crystal structures where the palladium atoms are exclusively surrounded by Ga atoms [34–36]. Because thermal stability and structural integrity of the intermetallic compounds under reaction conditions are prerequisites for the application as catalysts for the selective hydrogenation of acetylene, Part I of this paper series describes detailed structural investigations under inert, hydrogen and oxygen containing atmospheres as well as in the reactive feed with acetylene and hydrogen. *In situ* powder X-ray diffraction (XRD) and *in situ* X-ray absorption spectroscopy (EXAFS) were employed to study the long- and the short-range order in the crystal structures under reaction conditions, respectively. Part II focuses on the catalytic performance of the intermetallic compounds PdGa and Pd_3Ga_7 in the semi-hydrogenation of acetylene compared to Pd/Al_2O_3 and Pd–Ag alloy catalysts.

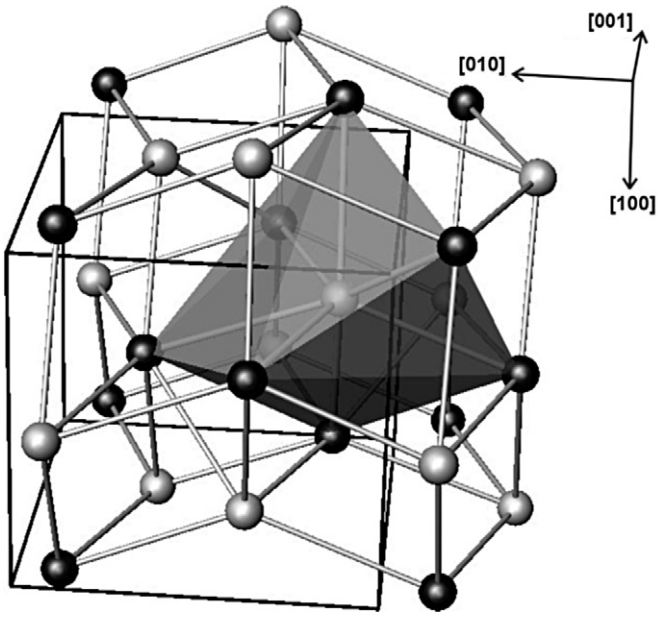

Fig. 1. In the crystal structure of PdGa each Pd atom (white spheres) is surrounded by seven Ga atoms (black spheres). The environment of one palladium atom is shown as polyhedron.

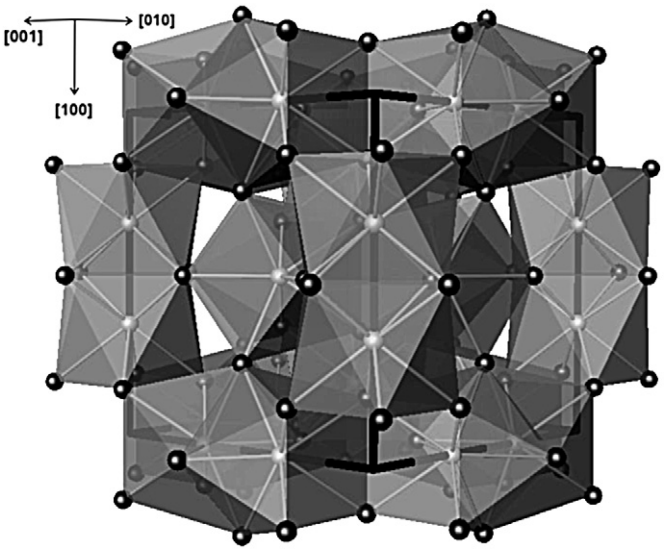

Fig. 2. The crystal structure of Pd_3Ga_7. Each Pd atom (white spheres) is surrounded by eight Ga atoms (black spheres) which form a square antiprism. The antiprisms are condensed to pairs via basal faces.

2. Experimental

2.1. Preparation of intermetallic compounds of palladium with gallium

Binary palladium–gallium intermetallic compounds were prepared by melting the corresponding amounts of Pd and Ga in glassy carbon crucibles under argon atmosphere in a high-frequency induction furnace [37]. 1.2083 g palladium (ChemPur 99.95%) and 0.7917 g gallium (ChemPur 99.99%) were used to obtain 2 g PdGa (11.35 mmol) while 0.7909 g Pd and 1.2091 g Ga yielded 2 g Pd_3Ga_7 (2.477 mmol). After the melting, Pd_3Ga_7 was annealed at 673 K for 800 h in a glassy carbon crucible, sealed in an evacuated quartz glass ampule, to obtain single-phase material. PdGa was used without further annealing. Both samples were powdered in a swing mill (Retsch MM 200, 4 ml WC pot, 2 WC balls, 25 Hz, air) for 2×30 min and 2×10 min for PdGa and Pd_3Ga_7, respectively. A more intensive milling procedure was used for PdGa compared to Pd_3Ga_7, because the particles of the latter seemed to agglomerate after extended milling.

2.2. Surface area characterization

The surface area of the intermetallic compounds was measured according to the BET method. Nitrogen adsorption experiments were performed using a Quantachrome Quantasorb Jr. The samples (2 g) were treated over night at 393 K in helium flow (20 ml/min) and measurements were performed by determining the total amount of nitrogen adsorbed using three different nitrogen concentrations.

Krypton adsorption experiments were performed using a BELSORP-max. The samples (400 mg) were pretreated in vacuum at 373 K for 1 h and measurements were performed by determining the total amount of Kr adsorbed using seven different krypton concentrations.

2.3. Thermal analysis

Thermal gravimetry (TG) and differential scanning calorimetry (DSC) measurements were performed on a Netzsch STA 449 C DSC/TG instrument. 30 mg of sample were employed and a gas phase composition of helium, 50% hydrogen in He, or 50% oxygen in He at a total flow of 100 ml/min and a heating rate of 6 K/min up to 723 K (PdGa) and 693 K (Pd_3Ga_7) was used. Prior to the measurements, the instrument was evacuated two times and, for the experiments in helium, it was additionally purged with helium over night (purity of all gases 5.0). An empty alumina crucible was used as reference.

2.4. Scanning electron microscopy

Scanning electron microscopy (SEM) was performed with a Hitachi S 4000 instrument equipped with an energy-dispersive X-ray detector (EDX) for elemental analysis. The acceleration voltage was set to 5 kV.

2.5. Powder X-ray diffraction

Ex situ powder X-ray diffraction patterns were measured by means of a STOE STADI P diffractometer (Cu$K_{\alpha 1}$ radiation, $\lambda = 1.540598$ Å, curved Ge monochromator) in transmission geometry with a linear position sensitive detector. *In situ* powder X-ray diffraction (XRD) experiments were conducted on a STOE diffractometer (CuK_α radiation, $\lambda = 1.54178$ Å) in Bragg–Brentano geometry equipped with a secondary monochromator, a scintillation counter, and a Bühler HDK high-temperature diffraction chamber mounted onto the goniometer. The gases were mixed by Bronkhorst mass-flow controllers and introduced in the experimental chamber with a total flow of 100 ml/min. The exhaust gas composition was continuously monitored with a mass spectrometer (QMS 200, Pfeiffer). For the *in situ* experiments usually 50 mg of the sample were dispersed onto a steel band. A detailed description of the setup used is published elsewhere [38].

The thermal stability of PdGa and Pd_3Ga_7 was studied in helium, 20% oxygen in He or 50% hydrogen in He. The XRD patterns for PdGa and Pd_3Ga_7 were measured in the 2θ range from 35.5° to 48.5° and from 22.5° to 52.5°, respectively, with a step width of 0.02° in 2θ and a counting time of 3 s/step. PdGa and Pd_3Ga_7 were heated from 323 to 723 K and from 323 to 693 K, respectively, and XRD patterns were measured isothermally every 50 K. The effective heating rate amounted to 0.5 K/min. Determination of the phase composition was aided by simulation of the theoretical patterns using the software PowderCell [39] and reference data from literature [35,36]. Crystallite sizes were calculated applying the Scherrer equation [40] using integral widths determined by fitting a pseudo-Voigt profile function to selected reflections with the program WinXAS 3.1 [41].

2.6. In situ EXAFS

In situ extended X-ray absorption fine structure (EXAFS) spectroscopy measurements were performed at HASYLAB beamline X1 (DESY, Hamburg, Germany) at the Pd K edge (24.350 keV). For the *in situ* EXAFS experiments a flow reactor [38] at atmospheric pressure in the transmission mode was used. The gas phase composition was continuously analyzed by mass spectrometry (Pfeiffer Omnistar). The samples (5 to 10 mg) were mixed with boron nitride (30 mg) and pressed into pellets with 5 mm in diameter at a force of 15 kN. Palladium foil was measured as reference for energy calibration. PdGa and Pd_3Ga_7 were heated at a rate of 6 K/min in helium, 50% oxygen in helium, 50% hydrogen in helium or a reaction gas mixture of 10% acetylene (2.6, Linde), 20% hydrogen and 70% helium.

Table 1
Coordination shells of Pd atoms in PdGa derived from crystal data [35] and selected structural parameters obtained by fitting a theoretical EXAFS function to the experimental EXAFS function $\chi(k)$ of PdGa at 300 K in 50% hydrogen in He (see also Fig. 6)

Shell	Element	CN[a]	Crystal data	EXAFS data		
			Distance (Å)	R (Å)	σ^2 (Å^2)	E_0 (eV)
1st	Ga	1	2.5371	2.52	0.008	−2.58
2nd	Ga	3	2.5669	2.55	0.008	−2.58
3rd	Ga	3	2.7038	2.68	0.007	−2.58
4th	Pd	6	3.0040	2.98	0.011	−3.12
5th	Ga	3	4.0029			
6th	Pd	6	4.3968			

[a] Coordination number.

Table 2
Coordination shells of Pd atoms in Pd_3Ga_7 based on crystallographic data [36] and selected structural parameters obtained by fitting the crystallographic data to the experimental EXAFS function $\chi(k)$ of Pd_3Ga_7 at 300 K in 50% hydrogen in He

Shell	Element	CN[a]	Crystal data	EXAFS data		
			Distance (Å)	R (Å)	σ^2 (Å^2)	E_0 (eV)
1st	Ga	4	2.5772	2.57	0.007	−0.65
2nd	Ga	4	2.5835	2.58	0.007	−0.65
3rd	Pd	1	2.7317	2.73	0.005	1.03
4th	Ga	4	4.1676			
5th	Pd	4	4.2709			
6th	Ga	4	4.4631			

[a] Coordination number.

Analysis of the EXAFS spectra was performed with the software WinXAS 3.1 [41]. After energy calibration, background correction, normalization and transformation into the k-space, an atomic background $\mu_0(k)$ was determined using a cubic spline function. The radial distribution function $FT(\chi(k) \times k^3)$ was obtained by Fourier transforming the k^3-weighted experimental $\chi(k)$ function (k range from 2 to 13 Å^{-1}), multiplied by a Bessel window, into the R space. Theoretical phases and amplitudes were calculated using FEFF 8 [42,43] for Pd–Ga and Pd–Pd scattering paths in the crystal structures of PdGa and Pd_3Ga_7. The EXAFS refinements were performed in R space to the k^2 and k^3 weighted experimental $FT(\chi(k))$ in a range from 1 to 5 Å. Fitting parameters were (i) Debye–Waller factors for all single scattering paths, (ii) distances of single scattering paths, (iii) two E_0 shifts for Pd–Pd and Pd–Ga shells and (iv) one 3rd cumulant for all scattering paths. Coordination numbers as well as the amplitude reduction factor S_0^2, which involves many-body effects, were kept invariant. Because of the small difference in the atomic distances of the first (1 Ga atom) and second Ga shell (3 Ga atoms) in PdGa (Table 1) the deviations from the crystallographic distances (R1 + 2) and the Debye–Waller factors (DW1 + 2) were correlated to be alike. Additionally, all higher Ga shells ($R = 4.0029$, 4.5732 and 4.6515 Å) and the higher Pd shells were correlated in the same way. Two multi-scattering paths ($R = 4.07$ and 4.13 Å) were included in the refinement. Accordingly, for the first and second Ga shell (4 Ga + 4 Ga atoms) in Pd_3Ga_7 (Table 2) the deviation from the crystallographic distances (R1 + 2) and the Debye–Waller factors (DW1 + 2) were also correlated to be alike. Four higher Ga shells ($R = 4.1676$ to 4.9019 Å) and two higher Pd shells ($R = 4.2709$ and 4.7923 Å) were correlated in the same way. Two additional multi-scattering paths ($R = 3.95$ and 4.71 Å) were included in the refinement. The estimated standard deviation of the determined distances is 0.02 Å. The Ga K edge XAFS data (10.367 keV) were measured as well but not employed for a structural refinement, because of the presence of gallium oxide on the surface (see TG, XPS and ISS data [44]), Ga-rich areas detected by EDX and two different crystallographic Ga sites in Pd_3Ga_7.

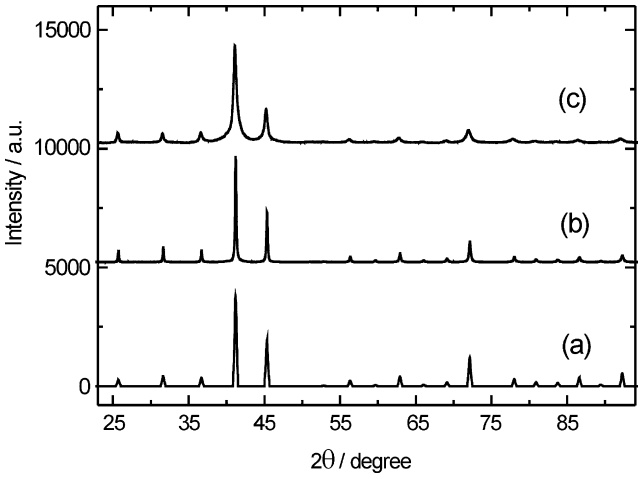

Fig. 3. Simulated (a) and experimental powder X-ray diffraction patterns of PdGa after grinding in a mortar (b) and after milling (c).

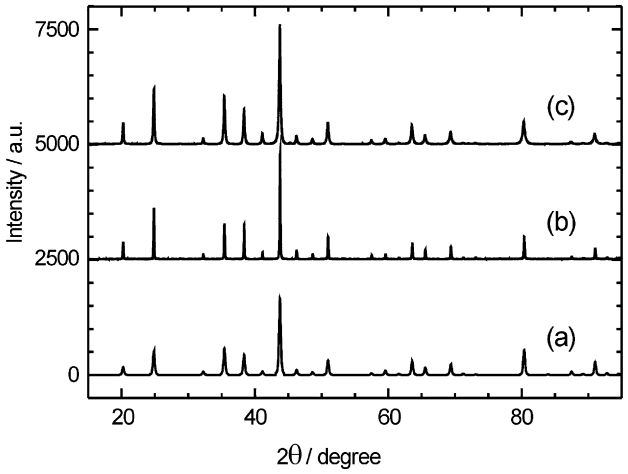

Fig. 4. Simulated (a) and experimental powder X-ray diffraction patterns of Pd_3Ga_7 after grinding in a mortar (b) and after milling (c).

3. Results and discussion

3.1. Structural characteristics of Pd–Ga intermetallic compounds

In PdGa and Pd_3Ga_7 the palladium atoms are only coordinated by Ga atoms in the first coordination shell and, hence, are effectively isolated from each other. PdGa [37] crystallizes in the FeSi type of crystal structure ($P2_13$, $a = 4.890$ Å) with each Pd atom coordinated by seven Ga atoms at distances between 2.537 and 2.704 Å (Table 1, Fig. 1). In contrast to Pd metal, which shows twelve neighboring Pd atoms at a distance of 2.744 Å, PdGa possesses only six neighboring Pd atoms at a significantly higher distance of 3.004 Å. In the gallium-richer Pd_3Ga_7 [36] ($Im\bar{3}m$, Ir_3Ge_7 type of crystal structure, $a = 8.7716$ Å) each Pd atom is coordinated by eight Ga atoms with an average distance of 2.5804 Å and by one Pd atom at a distance of 2.7317 Å (Table 2, Fig. 2).

3.2. Characterization and pretreatment of PdGa and Pd_3Ga_7

As-prepared PdGa and Pd_3Ga_7 were ground in a mortar and the single-phase character was confirmed by *ex situ* powder X-ray diffraction. The experimental XRD pattern showed no deviation from the calculated diffraction pattern of PdGa [35] (Fig. 3) and Pd_3Ga_7 [36] (Fig. 4).

To increase the surface area, the materials were treated in a swing mill. XRD patterns of the milled samples showed also no change in the phase composition but a significant increase in the full width at half maximum (FWHM) of the peaks which indicated a reduction of the crystallite size (17.5 nm for PdGa and 34.0 nm for Pd_3Ga_7). Nitrogen adsorption measurements of both samples after milling resulted in BET surface areas of less than 0.5 $m^2\,g^{-1}$. Samples were subjected to krypton BET measurements to get more precise values of the surface area, revealing surface areas of 0.08 and 0.41 $m^2\,g^{-1}$ for ground and milled PdGa, respectively. In the case of Pd_3Ga_7 the determined surface area for a ground sample was 0.18 $m^2\,g^{-1}$, while a milled sample showed 0.37 $m^2\,g^{-1}$.

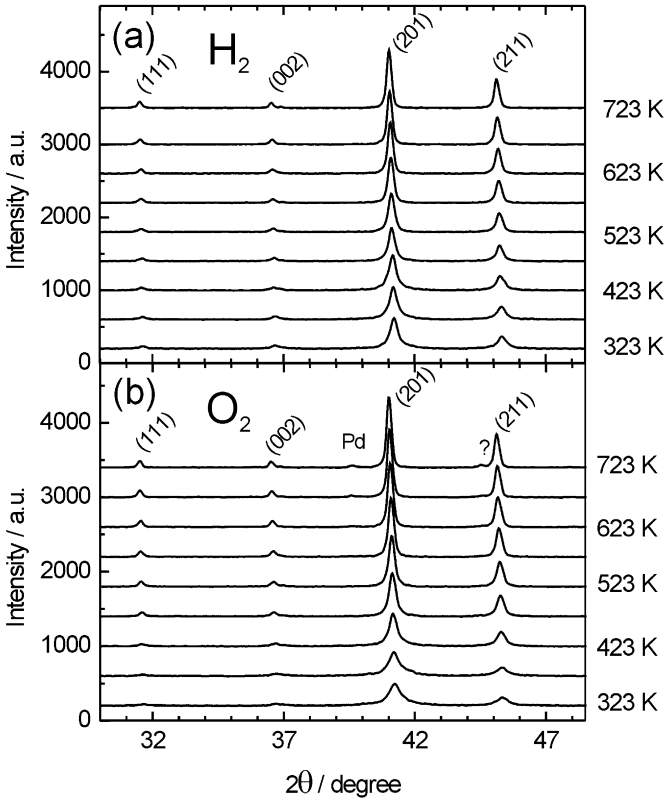

Fig. 5. Evolution of *in situ* X-ray diffraction patterns measured during thermal treatment of PdGa from 323 to 723 K: (a) in 50% hydrogen in helium and (b) in 20% oxygen in helium.

3.3. Thermal stability in reactive atmospheres

In the absence of reactive gases PdGa melts congruently at 1318 K and Pd_3Ga_7 forms peritectically at 733 K [34]. Since during the hydrogenation of acetylene, H_2 and C_2H_2 are present and a treatment with O_2 may be needed to reactivate the compounds after some time on stream, gravimetric analysis in oxidizing and reducing atmospheres as well as *in situ* powder X-ray diffraction and *in situ* EXAFS were performed on PdGa and Pd_3Ga_7.

3.4. In situ XRD

In situ XRD patterns measured during thermal treatment of PdGa in 50% hydrogen in helium and in 20% oxygen in He (to check the stability of the compound under regeneration conditions) are shown in Figs. 5a and 5b, respectively. No additional diffraction lines corresponding to Pd metal, PdO or Ga_2O_3 were detected in the temperature range employed for the hydrogen containing atmosphere. In a mixture of 20% oxygen in helium, the formation of a peak at $2\theta = 39.7°$ at 623 K indicates the presence of small amounts of Pd metal, formed by decomposition of PdO [45]. An additional peak at $2\theta = 44.5°$ formed at 673 K could not be identified

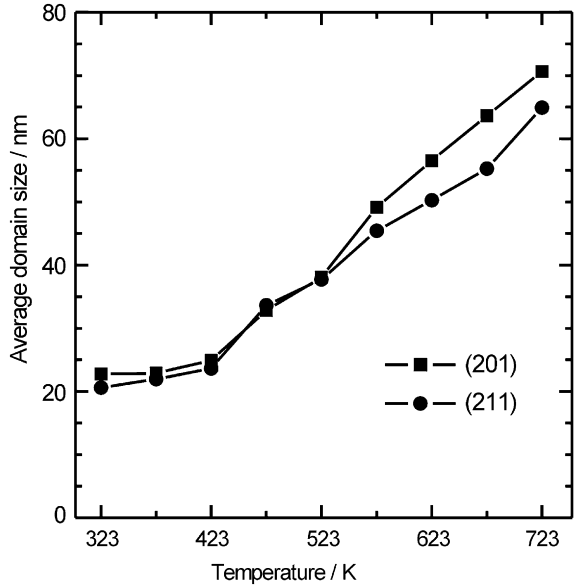

Fig. 6. Evolution of average domain size of PdGa during thermal treatment in 50% hydrogen in helium obtained from by profile analysis of (201) and (211) reflections.

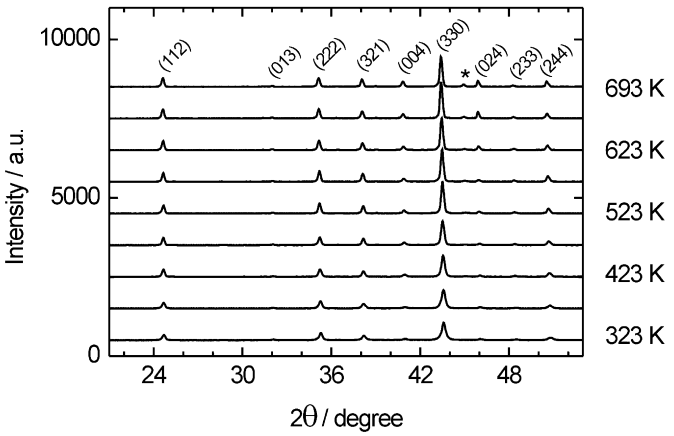

Fig. 7. Evolution of *in situ* X-ray diffraction patterns measured during thermal treatment of Pd_3Ga_7 in 50% hydrogen in helium from 323 to 693 K. Formation of PdGa at high temperatures is observed (*).

within the systems Pd–Ga, Pd–H, Pd–O, Ga–O and Pd–Ga–O. A significant narrowing of the diffraction lines with temperature can be observed indicative of crystallite growth and sintering of the milled material. Profile fitting of the (201) and (211) reflections of PdGa results in an average crystallite size of 18 nm for ball-milled PdGa while the average crystallite size increases to 70 nm at 723 K (Fig. 6) during thermal treatment. The linear shift of 0.2° in 2θ of the (201) reflection with increasing temperature in helium, oxygen as well as hydrogen is attributed to the thermal expansion of the compound. Because of the alike behavior of PdGa in the different atmospheres the incorporation of hydrogen or oxygen in the bulk structure can be excluded.

In situ XRD patterns measured during the thermal treatment of Pd_3Ga_7 in 50% hydrogen in helium are shown in Fig. 7. The small additional peak at $2\theta = 45.3°$ (indicated by *) appears at 523 K in helium and oxygen atmospheres as well as at 573 K in hydrogen and is indicative for the formation of PdGa during the thermal treatment by peritectic decomposition of Pd_3Ga_7 [34]. The most intense reflection (201) of PdGa is not observed due to overlap with the (004) reflection of Pd_3Ga_7. Rietveld refinement of the experimental powder X-ray diffraction patterns at 693 K yields an amount of 5 wt% of PdGa with no additional phases detectable. Refinement of the powder patterns after cooling to ambient temperature resulted in a composition of 91% (hydrogen atmosphere) and 88% (oxygen and helium atmospheres) Pd_3Ga_7 together with PdGa. As in the case of PdGa, the decrease of 0.2° in 2θ of the (330) diffraction line of Pd_3Ga_7 with temperature in helium, oxygen and hydrogen is attributed to the thermal expansion of the Pd_3Ga_7 lattice. Profile fitting of the (321) reflection of Pd_3Ga_7 yielded a crystallite size of 34 nm for ball-milled Pd_3Ga_7 and 100 nm for Pd_3Ga_7 at 693 K.

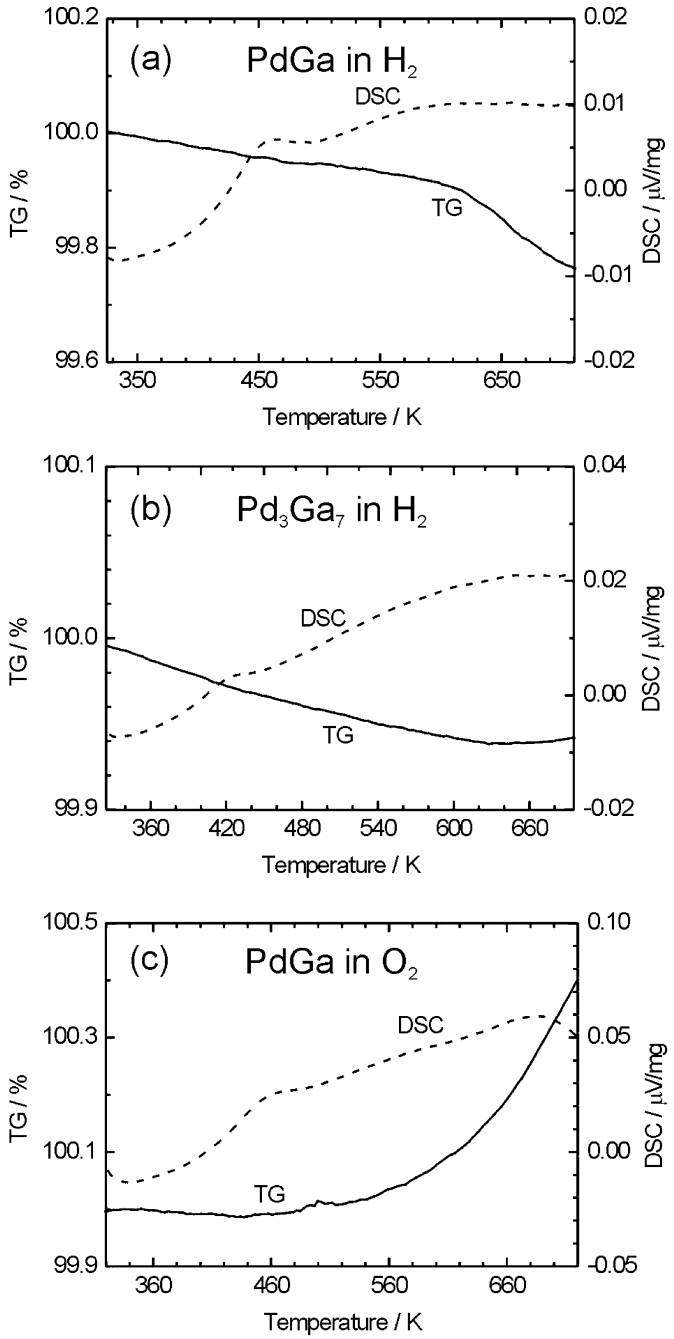

Fig. 8. Relative mass TG (solid) and DSC signal (dashed) during thermal treatment of: (a) PdGa in 50% hydrogen in helium (300 to 723 K at 6 K/min); (b) Pd_3Ga_7 in 50% hydrogen in helium (300 to 693 K at 6 K/min); (c) PdGa in 50% oxygen in helium (300 to 723 K at 6 K/min).

3.5. Thermal analysis

DSC/TG revealed a considerable stability of the materials up to 600 and 550 K, respectively, in reducing (H_2) and oxidizing (O_2) atmospheres. During the treatment in 50% hydrogen in helium, PdGa showed only a very small mass loss in the range from 300 to 600 K possibly because of the desorption of water and/or CO_2, or slight reduction of a surface oxide (Fig. 8a). A more pronounced mass loss at ~600 K indicates the onset of a significant surface oxide reduction. Pd_3Ga_7 showed an even smaller mass loss in the range from 300 to 620 K indicating only slight contributions of oxide reduction in the temperature range employed (Fig. 8b). Given the overall lower stability of Pd_3Ga_7 compared to PdGa, this effect may be caused by the smaller surface area of Pd_3Ga_7 as a result of the less intensive ball milling employed. During treatment in 50% oxygen in He, PdGa showed a mass gain at 500 K (onset temperature) indicating oxidation of the material (Fig. 8c). Pd_3Ga_7 showed a similar behavior during the treatment in oxygen. The DSC traces measured of the two materials under reducing and oxidizing atmospheres exhibited small exothermic peaks at about 420 and 460 K for Pd_3Ga_7 and PdGa, respectively. No hints for hydride or carbide formation, phase transitions or decomposition of the compounds were observed. The small exothermic DSC signal detected at ~460 K during treatment of PdGa in hydrogen and oxygen (Figs. 5a and 5b) and at ~420 K during treatment of Pd_3Ga_7 in hydrogen (Fig. 8c) may indicate sintering of the milled intermetallic compounds. This is in good agreement with the onset of crystallite growth of PdGa at ~460 K during treatment in hydrogen as determined by *in situ* XRD (Fig. 6) and can also be observed in the trend of the Debye–Waller factors (see below, Fig. 12).

3.6. Scanning electron microscopy

Scanning electron microscopy images of PdGa after ball milling and after subsequent treatment in 50% hydrogen in helium for 30 min at 573 K are depicted in Fig. 9. Pd_3Ga_7 showed a similar morphology and behavior. The ball milled sample exhibited particles sizes and agglomerates in the range of 2 to 20 µm (Fig. 9a) with Pd_3Ga_7 having a slightly larger average particle size than PdGa (not shown). EDX measurements show a homogeneous composition of the particles before and after heating in hydrogen except for a few regions with higher Ga content. After treatment in hydrogen at 573 K the particles appeared to be slightly more coalesced and exhibited smoother surfaces (Fig. 9b). The regions with higher Ga content persisted.

3.7. In situ EXAFS

In situ EXAFS studies on PdGa and Pd_3Ga_7 were performed during thermal treatment in helium, 50% hydrogen in He or a mixture of 10% acetylene and 20% hydrogen in helium. Fig. 10 shows the experimental $FT(\chi(k)\times k^3)$ of PdGa in 50% hydrogen at 300 K together with the theoretical $FT(\chi(k)\times k^3)$ obtained by the refinement procedure described above. The $FT(\chi(k)\times k^3)$ shows two main maxima at 2.2 and 2.8 Å. The first maximum can be assigned to the three Ga shells and the second maximum to the first Pd shell. A good agreement between the experimental and theoretical $FT(\chi(k)\times k^3)$ can be seen and the interatomic distances obtained (Table 1) show only minor deviations from the crystallographic data. The low Debye–Waller factors indicate a highly ordered structure of PdGa. No expansion of interatomic distances or structural disorder, indicating the incorporation of hydrogen or carbon, is detected. The evolution of the $FT(\chi(k)\times k^3)$ of PdGa during treatment in 50% hydrogen in helium from 300 to 723 K is depicted in

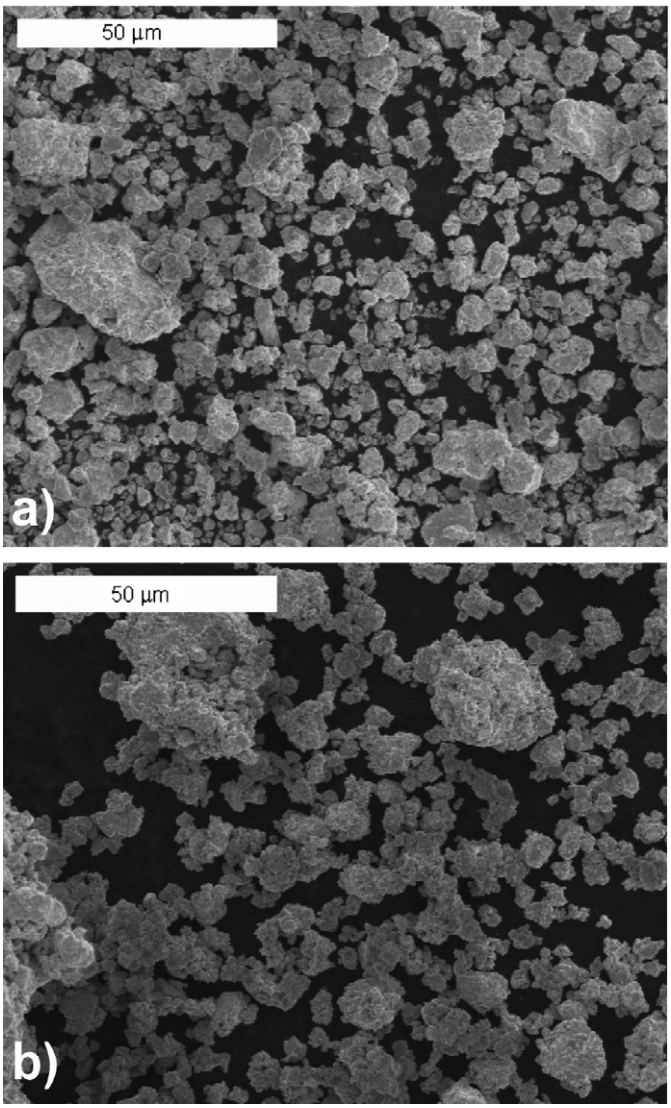

Fig. 9. Scanning electron microscopy images of milled PdGa: (a) before; (b) after heating in 50% hydrogen in helium to 573 K for 30 min.

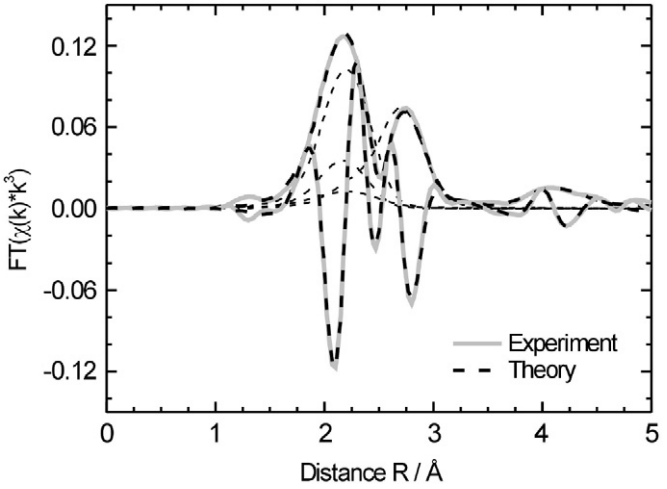

Fig. 10. Experimental (gray and solid lines) and theoretical (black and dashed line) Pd K edge $FT(\chi(k)\times k^3)$ of PdGa at 300 K in 50% hydrogen in helium.

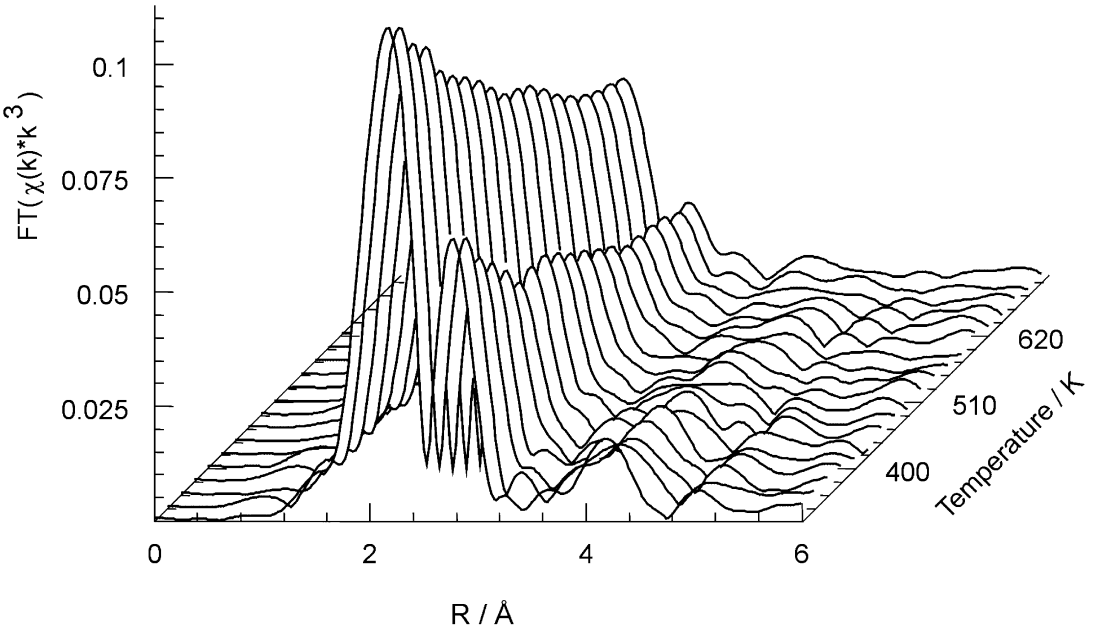

Fig. 11. Evolution of Pd K edge $FT(\chi(k) \times k^3)$ measured during thermal treatment of PdGa in 50% hydrogen in helium from 300 to 723 K.

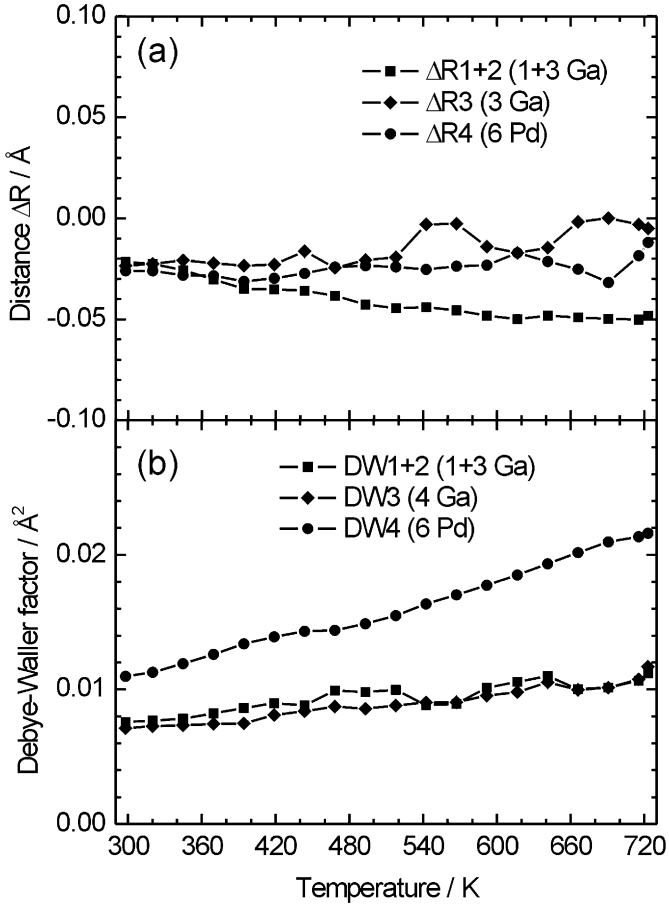

Fig. 12. Evolution of (a) selected relative Pd–Ga and Pd–Pd distances and (b) Debye–Waller factors of selected scattering paths of PdGa during thermal treatment of PdGa in 50% hydrogen in helium from 323 to 723 K obtained from analysis of the corresponding XAFS spectra.

Fig. 11. The overall decrease in amplitude of the $FT(\chi(k) \times k^3)$ is caused by an increasing thermal disorder during heating.

The characteristic distances of PdGa heated in hydrogen, helium, oxygen and in reaction feed (containing acetylene and hydrogen) obtained from the EXAFS analysis remain nearly constant over the temperature range employed (Fig. 12a). The Debye–Waller factors of three selected shells exhibit the expected nearly linear increase with temperature (Fig. 12b). Smaller changes in the trend of distances and a more linear behavior of Debye–Waller factors for Pd_3Ga_7 compared to PdGa is observed during treatment in hydrogen, helium and oxygen. No structural changes that can be attributed to phase transitions, formation of hydrides or carbides or the incorporation of hydrogen were detected during the thermal treatment in the various atmospheres employed. In the acetylene hydrogenation feed, PdGa and Pd_3Ga_7 showed a similar behavior compared to the treatment of the materials in hydrogen. The onset of catalytic activity (see Part II [44]) of both materials did not correlate with changes in the long-range (XRD) or short-range (EXAFS) order.

3.8. Incorporation of hydrogen and carbon in palladium hydrogenation catalysts

In addition to being effected by the presence of neighboring Pd sites on the catalyst surface, the limited selectivity and long-term stability of palladium in acetylene hydrogenation is caused by the formation of palladium hydrides under reaction conditions. It has been reported that the formation of β-palladium hydride may decrease the selectivity to ethylene by enhancing the complete hydrogenation of acetylene [2,17]. This effect has been ascribed to a higher concentration of surface hydrogen in β-palladium hydride [18]. Doyle et al. have shown that hydrogenation of alkenes requires the formation of weakly bonded subsurface hydrogen [19] and Teschner et al. very recently investigated the influence of subsurface hydrogen on the selectivity of the semi-hydrogenation of alkynes [46]. Apparently, materials that do not exhibit the formation of hydrides should possess a limited availability of hydrogen

from the bulk, which should result in an improved selectivity. In combination with the absence of hydrogen in the catalyst bulk, isolating Pd atoms on the catalyst surface will reduce the number of adsorption and dissociation sites for hydrogen and thereby further diminish the hydrogen supply for the unwanted ethylene hydrogenation [20,24]. As has been shown by Teschner et al. by *in situ* XPS measurements, metallic Pd is building up a surface Pd/C phase (BE 335.6 eV) during the partial hydrogenation of pentyne which fulfills two purposes: (a) it prevents the dissolved hydrogen from reaching the surface, preventing it to take part in the hydrogenation, thus, leading to higher selectivity and (b) being the actually active species for the partial hydrogenation of the C≡C bond [47–49].

The changes in the electronic structure of elemental Pd by incorporation of C are very similar to the changes that Pd undergoes by the formation of Pd/Ga intermetallic compounds, according to XPS studies [6,50]. The examined palladium containing intermetallic compounds show no detectable incorporation of hydrogen or carbon in the bulk and, hence, should show a reduced surface concentration of hydrogen under reaction conditions and an increased selectivity [20–24]. The incorporation of hydrogen or carbon in palladium metal as well as the formation of hydrides, results in an expansion of the crystallographic unit cell and increased interatomic distances [51,52]. Both effects should be detectable by *in situ* XRD and *in situ* XAFS [53–55]. *In situ* XRD patterns of PdGa and Pd_3Ga_7 measured under reaction conditions showed only a small and linear peak shift towards lower diffraction angles, i.e. larger unit cells (Figs. 5 and 7). While the lattice expansion due to hydride formation as well as the thermal lattice expansion will result in a shift of the diffraction peaks to lower angles, the thermal expansion results in a linear peak shift with temperature, independent from the gas atmosphere. From the linear increase of the distances with temperature observed in the *in situ* XRD and EXAFS data (Fig. 12) under all tested atmospheres, it can be concluded that the intermetallic compounds form no detectable amount of hydrides under reaction conditions. Similar to the incorporation of hydrogen in the lattice of the intermetallic compounds, no formation of a carbon containing phase under acetylene reaction conditions was detected.

The observed high structural stability of PdGa and Pd_3Ga_7 can be attributed to pronounced covalent bonding (localized by means of the electron localization function) in both crystal structures supporting strongly the site isolation approach [6,50]. Therefore, it is essential to apply intermetallic compounds rather than alloys for the concept of active-site isolation. The covalent bonding present in PdGa and Pd_3Ga_7 accounts for the remarkable stability against continuous chemical induced segregation and the suppression of the formation of a highly reactive hydride phases, which results in an improved selectivity in the hydrogenation of acetylene. From our investigations, it appears advisable to keep the reaction and regeneration temperature below 473 K to avoid significant sintering, oxidation and loss of active catalyst surface.

4. Conclusions

The palladium–gallium intermetallic compounds PdGa and Pd_3Ga_7 are introduced as selective catalysts for the hydrogenation of acetylene. The compounds can readily be prepared by thermal treatment of stoichiometric mixtures of the corresponding metals. The initially low surface area of the as-prepared materials can be increased by careful mechanical treatment without decomposition or loss of structural order. The compounds possess well-defined crystallographic structures in which the Pd atoms are only coordinated by Ga atoms in the first coordination shell, thus, effectively isolating the Pd atoms from each other. This is a clear difference to the randomly distributed Pd atoms in binary alloy clusters as introduced by Sinfelt. The ordered crystal structures shall permit to investigate the concept of active-site isolation in hydrogenation catalysis and its beneficiary effect on selectivity and long-term stability. Furthermore the partly covalent bonding inhibits the subsurface chemistry, thus being very different to elemental Pd, where a Pd/C phase is the catalytic species for the partial hydrogenation of alkynes.

Detailed *in situ* investigations of PdGa and Pd_3Ga_7 by DSC/TG, XRD and EXAFS during thermal treatment under various inert or reactive gas atmospheres showed that the long- and short-range ordered crystal structures of the materials are intact up to 600 K. No phase transitions, decomposition, segregation or incorporation of hydrogen or carbon were detected. The observed remarkable stability is due to the partly covalent bonding between Pd and Ga and, hence, the structural motive of isolated Pd active-sites is preserved under hydrogenation reaction conditions.

Both intermetallic compounds studied exhibit sufficient thermal stability as well as isolation of Pd centers under reaction conditions. Accordingly, palladium–gallium intermetallic compounds may not only be interesting model systems for the selective hydrogenation, but also promising candidates for technical applications.

Acknowledgments

We acknowledge HASYLAB Hamburg for providing beamtime and J. Wienold for assisting at beamline X1. We thank Gisela Weinberg for performing SEM and EDX measurements. Fruitful discussions within the ATHENA project are gratefully acknowledged.

Supporting information

The online version of this article contains additional supplementary material.

Please visit DOI: 10.1016/j.jcis.2008.06.013.

References

[1] A.N.R. Bos, K.R. Westerterp, Chem. Eng. Process. 32 (1993) 1.
[2] A. Borodzinski, G.C. Bond, Catal. Rev. 48 (2006) 91.
[3] H. Arnold, F. Döbert, J. Gaube, in: G. Ertl, H. Knözinger, J. Weitkamp (Eds.), Handbook of Heterogeneous Catalysis, VCH, Weinheim, 1997, p. 2165.
[4] A. Molnar, A. Sarkany, M. Varga, J. Mol. Catal. A Chem. 173 (2001) 185.
[5] P. Albers, J. Pietsch, S.F. Parker, J. Mol. Catal. A Chem. 173 (2001) 275.
[6] K. Kovnir, M. Armbrüster, J. Osswald, T. Ressler, R.E. Jentoft, R. Giedigkeit, Yu. Grin, R. Schlögl, Angew. Chem. (2007), submitted for publication.
[7] E.G. Derouane, J. Mol. Catal. 25 (1984) 51.
[8] E.W. Shin, C.H. Choi, K.S. Chang, Y.H. Na, S.H. Moon, Catal. Today 44 (1998) 137.
[9] S. Leviness, V. Nair, A.H. Weiss, Z. Schay, L. Guczi, J. Mol. Catal. 25 (1984) 131.
[10] V. Ponec, Adv. Catal. 32 (1983) 149.
[11] W. Palczewska, A. Jablonski, Z. Kaszkur, G. Zuba, J. Wernisch, J. Mol. Catal. 25 (1984) 307.
[12] Y.M. Jin, A.K. Datye, E. Rightor, R. Gulotty, W. Waterman, M. Smith, M. Holbrook, J. Maj, J. Blackson, J. Catal. 203 (2001) 292.
[13] J.H. Kang, E.W. Shin, W.J. Kim, J.D. Park, S.H. Moon, J. Catal. 208 (2002) 310.
[14] J.W. Medlin, M.D. Allendorf, J. Phys. Chem. B 107 (2003) 217.
[15] C.J. Baddeley, A.F. Lee, R.M. Lambert, T. Giessel, O. Schaff, V. Fernandez, K.M. Schindler, A. Theobald, C.J. Hirschmugl, R. Lindsay, A.M. Bradshaw, D.P. Woodruff, Surf. Sci. 400 (1998) 166.
[16] A. Valcarcel, A. Clotet, J.M. Ricart, F. Illas, Chem. Phys. 309 (2005) 33.
[17] W. Palczewska, in: Z. Paal, P.G. Denon (Eds.), Hydrogen Effects in Catalysis, Marcel Decker, New York, 1988, p. 372.
[18] G.C. Bond, P.B. Wells, J. Catal. 5 (1966) 65.
[19] A.M. Doyle, S.K. Shaikhutdinov, S.D. Jackson, H.J. Freund, Angew. Chem. Int. Ed. 42 (2003) 5240.
[20] A.S. McLeod, R. Blackwell, Chem. Eng. Sci. 59 (2004) 4715.
[21] C.M. Pradier, M. Mazina, Y. Berthier, J. Oudar, J. Mol. Catal. 89 (1994) 211.
[22] T. Komatsu, S. Hyodo, T. Yashima, J. Phys. Chem. B 101 (1997) 5565.
[23] Q.W. Zhang, J. Li, X.X. Liu, Q.M. Zhu, Appl. Catal. A 197 (2000) 221.
[24] M. Morkel, G. Rupprechter, H.J. Freund, Surf. Sci. 588 (2005) L209.
[25] M.M. Johnson, D.W. Walker, G.P. Nowack, US Patent 4404124, 1983.
[26] B. Coq, F. Figueras, J. Mol. Catal. A Chem. 173 (2001) 117.
[27] L. Guczi, J. Mol. Catal. 25 (1984) 13.
[28] W.M.H. Sachtler, J. Mol. Catal. 25 (1984) 1.

[29] O.M. Lovvik, Surf. Sci. 583 (2005) 100.
[30] J.L. Rousset, J.C. Bertolini, P. Miegge, Phys. Rev. B 53 (1996) 4947.
[31] B.E. Nieuwenhuys, Surf. Rev. Lett. 3 (1996) 1869.
[32] J.H. Sinfelt, Sci. Am. 253 (1985) 90.
[33] G. Meitzner, G.H. Via, F.W. Lytle, J.H. Sinfelt, J. Chem. Phys. 87 (1987) 6354.
[34] T.B. Massalski, Binary Alloy Phase Diagrams, second ed., ASM International, Ohio, USA, 1990.
[35] M.K. Bhargava, A.A. Gadalla, K. Schubert, J. Less-Common Met. 42 (1975) 76.
[36] K. Khalaff, K. Schubert, J. Less-Common Met. 37 (1974) 129.
[37] R. Giedigkeit, Intermetallische Verbindungen im System Yb–Pd–Ga, Diploma Thesis, Technische Universität Darmstadt, 1998.
[38] T. Ressler, R.E. Jentoft, J. Wienold, M.M. Günter, O. Timpe, J. Phys. Chem. B 104 (2000) 6360.
[39] W. Kraus, G. Nolze, PowderCell for Windows 2.4, Federal Institute for Material Research and Testing, Germany, 2000.
[40] R.A. Young, The Rietveld Method, Oxford Univ. Press, Oxford, 1993.
[41] T. Ressler, J. Synch. Radiat. 5 (1998) 118.
[42] J.J. Rehr, R.C. Albers, Phys. Rev. B 41 (1990) 8139.
[43] A.L. Ankudinov, B. Ravel, J.J. Rehr, S.D. Conradson, Phys. Rev. B 58 (1998) 7565.
[44] J. Osswald, K. Kovnir, M. Armbrüster, R. Giedigkeit, R.E. Jentoft, U. Wild, Yu. Grin, R. Schlögl, J. Catal. 258 (2008) 219, Part II of this study.
[45] E. Rey, M.R. Kamal, R.B. Miles, B.S.H. Royce, J. Mater. Sci. 13 (1978) 812.
[46] D. Teschner, J. Borsodi, A. Wootsch, Z. Révay, M. Hävecker, A. Knop-Gericke, S.D. Jackson, R. Schlögl, Science 320 (2008) 86.
[47] D. Teschner, A. Pestryakov, E. Kleimenov, M. Hävecker, H. Bluhm, H. Sauer, A. Knop-Gericke, R. Schlögl, J. Catal. 230 (2005) 186.
[48] D. Teschner, A. Pestryakov, E. Kleimenov, M. Hävecker, H. Bluhm, H. Sauer, A. Knop-Gericke, R. Schlögl, J. Catal. 230 (2005) 195.
[49] D. Teschner, E. Vass, M. Hävecker, S. Zafeiratos, P. Schnörch, H. Sauer, A. Knop-Gericke, R. Schlögl, M. Chamam, A. Wootsch, A.S. Canning, J.J. Gamman, S.D. Jackson, J. McGregor, L.F. Gladden, J. Catal. 242 (2006) 26.
[50] K. Kovnir, M. Armbrüster, D. Teschner, T.V. Venkov, F.C. Jentoft, A. Knop-Gericke, Yu. Grin, R. Schlögl, Sci. Technol. Adv. Mater. 8 (2007) 420–427.
[51] F.A. Lewis, The Palladium Hydrogen System, Academic Press, London, 1967.
[52] A. Frąckiewicz, A. Janko, Acta Crystallogr. A 34 (1978) S377.
[53] A. Rose, S. Maniguet, R.J. Mathew, C. Slater, J. Yao, A.E. Russell, Phys. Chem. Chem. Phys. 5 (2003) 3220.
[54] N.K. Nag, J. Phys. Chem. B 105 (2001) 5945.
[55] A.E. Russell, S. Maniguet, R.J. Mathew, J. Yao, M.A. Roberts, D. Thompsett, J. Power Sources 96 (2001) 226.